AGU PUBLICATIONS

Geophysical Research Letters

RESEARCH LETTER
10.1002/2014GL060321

Key Points:
- Hosing experiments with CCSM3 under Marine Isotope Stage 3 conditions
- A highly unstable AMOC is simulated in a state-of-the-art climate model
- Minor freshwater fluxes trigger Dansgaard-Oeschger type climate shifts

Supporting Information:
- Readme
- Figures S1–S4

Correspondence to:
X. Zhang,
xzhang@marum.de

Citation:
Zhang, X., M. Prange, U. Merkel, and M. Schulz (2014), Instability of the Atlantic overturning circulation during Marine Isotope Stage 3, *Geophys. Res. Lett.*, *41*, doi:10.1002/2014GL060321.

Received 28 APR 2014
Accepted 2 JUN 2014
Accepted article online 6 JUN 2014

Instability of the Atlantic overturning circulation during Marine Isotope Stage 3

Xiao Zhang[1], Matthias Prange[1], Ute Merkel[1], and Michael Schulz[1]

[1]MARUM—Center for Marine Environmental Sciences and Faculty of Geosciences, University of Bremen, Bremen, Germany

Abstract Variations in the strength of the Atlantic meridional overturning circulation (AMOC) were involved in the occurrences of Dansgaard-Oeschger (D-O) events during Marine Isotope Stage 3 (MIS3). The stability of the AMOC to North Atlantic freshwater perturbations is studied using a comprehensive climate model under MIS3 boundary conditions. An AMOC stability diagram constructed from a series of equilibrium freshwater perturbation experiments reveals a highly nonlinear dependence of AMOC strength on freshwater forcing. The MIS3 baseline state is remarkably unstable with respect to minor perturbations. The global climate signal associated with a change in AMOC strength is consistent with a transition from an interstadial to a stadial state including an annual mean surface air temperature drop of ~8 K in central Greenland. We suggest that minor freshwater perturbations in the hydrologic cycle, e.g., related to ice sheet processes, had the potential to trigger D-O-type climate shifts associated with a threshold in the atmosphere-ocean system.

1. Introduction

Marine Isotope Stage 3 (MIS3, 57–29 ka B.P.) was a period of pronounced millennial-scale climate variability, associated with the most regular occurrence of Dansgaard-Oeschger (D-O) events [*Schulz*, 2002]. Characterized by rapid transitions between cold stadials and warm interstadials at northern latitudes [*Dansgaard et al.*, 1993; *Bond et al.*, 1993], the significance of D-O events is substantiated by global-scale climate variations that can be correlated to the Greenland temperature record [*Broecker*, 2000; *Voelker and workshop participants*, 2002; *EPICA community members*, 2006]. The origin of D-O events is still a matter of controversy [*Timmermann et al.*, 2003], but there is strong evidence that variations in the strength of the Atlantic meridional overturning circulation (AMOC) and its associated heat transport were involved, where strong (weak) overturning is related to interstadial (stadial) climate, although these D-O-type AMOC variations were probably much smaller than those associated with Heinrich events [*Keigwin and Boyle*, 1999; *van Kreveld et al.*, 2000; *Sarnthein et al.*, 2001; *Elliot et al.*, 2002; *Clement and Peterson*, 2008]. A widely held view of D-O dynamics involves switches between two stable states of different AMOC strength. Accordingly, numerous conceptual models have been suggested to explain the millennial-scale climate oscillations based on the concept of oceanic bistability [e.g., *Stocker and Wright*, 1991; *Timmermann et al.*, 2003; *Sarnthein et al.*, 2001; *Clement and Peterson*, 2008; *Colin de Verdière et al.*, 2006]. Meltwater injections into the Nordic Seas associated with internal northern ice sheet dynamics have been suggested as a potential pacemaker for AMOC state transitions and associated D-O climate oscillations [*van Kreveld et al.*, 2000]. Understanding the stability properties of the glacial ocean circulation to freshwater perturbations is therefore key toward an understanding of D-O climate variability.

Important insights into the potential dynamics of D-O events were provided by simulations with the Earth system model of intermediate complexity (EMIC) CLIMBER-2 [*Ganopolski and Rahmstorf*, 2001]. It has been shown that the stability properties of the AMOC under glacial boundary conditions may differ fundamentally from the interglacial case. In particular, CLIMBER-2 suggested the existence of two modes of the AMOC in close proximity to the unperturbed glacial state and that minor freshwater perturbations can trigger transitions between these two modes causing D-O-type climate variations. It is known, however, that AMOC stability properties are model dependent [e.g., *Rahmstorf et al.*, 2005; *Stouffer et al.*, 2006], and it is therefore unclear to which extent the EMIC-based results are robust in the framework of more complex models. While various EMICs have been employed to study abrupt climate change associated with AMOC stability properties specific to the last glaciation [*Prange et al.*, 2002; *Schmittner et al.*, 2002; *van Meerbeeck et al.*, 2009; *Montoya and Levermann*, 2008; *Knorr and Lohmann*, 2003; *Banderas et al.*, 2012], so far no attempts have been made to systematically examine AMOC stability in a comprehensive coupled general circulation model under MIS3 boundary conditions. Here we present results from a series of quasi-equilibrium freshwater-hosing/extraction

experiments using the Community Climate System Model version 3 (CCSM3) forced with MIS3 boundary conditions and varying North Atlantic freshwater perturbations to assess the stability properties of the ocean circulation and its potential role in D-O climate variability.

2. Experimental Design

NCAR's (National Center for Atmospheric Research) CCSM3 is a fully coupled comprehensive general circulation model, composed of four separate components representing atmosphere, ocean, land, and sea ice [*Collins et al*., 2006]. In our simulations, the resolution of the atmospheric component is given by T31 (3.75° transform grid) with 26 layers in the vertical, while the ocean has a nominal resolution of 3° with equatorial grid refinement in meridional direction (down to 0.9°) and 25 levels in the vertical [*Yeager et al*., 2006]. The land model is defined on the same horizontal grid as the atmosphere and includes components for biogeophysics, biogeochemistry, and the hydrologic cycle as well as an interactive dynamic global vegetation model [*Oleson et al*., 2004; *Levis et al*., 2004]. In order to improve the simulation of the land surface hydrology and vegetation cover, new parameterizations for canopy interception and soil evaporation have been implemented into the land component [*Oleson et al*., 2008], identical to the model design used in a previous study [*Handiani et al*., 2013].

Along with a 1000 year integrated preindustrial control run, we performed a MIS3 baseline simulation applying 38 ka B.P. orbital forcing [*Berger*, 1978] and corresponding greenhouse gas concentrations of CO_2 (215 ppmv), CH_4 (501 ppbv), and N_2O (234 ppbv) [*Flückiger et al*., 2004; *Spahni et al*., 2005; *Ahn and Brook*, 2007; *Bereiter et al*., 2012]. In addition, the 38 ka B.P. ICE-5G continental ice sheet distribution has been implemented [*Peltier*, 2004], and the correspondingly reduced sea level results in a modified land-sea distribution (e.g., closing of the Bering Strait). The MIS3 baseline simulation was initialized with the final state of a 1500 years long simulation with LGM (Last Glacial Maximum, 21 ka B.P.) boundary conditions and integrated for another 2170 years. Note that this MIS3 simulation differs from a previous CCSM3 MIS3 experiment with the same resolution [*Merkel et al*., 2010] by the choice of the time slice, the implementation of a dynamic vegetation module, changes in the parameterizations for canopy interception and soil evaporation, and the integration length. The 38 ka time slice was chosen because it lies right in the middle of a rather regular sequence of D-O cycles and coincides with Heinrich event 4 [*Hemming*, 2004].

Branching off from year 1670 of the MIS3 simulation, we performed 12 freshwater-hosing/extraction experiments with different rates of continuous, unbalanced freshwater surface flux (treated as a virtual salinity flux [e.g., *Prange and Gerdes*, 2006] in CCSM3) homogeneously distributed over the Nordic Seas [cf. *van Kreveld et al*., 2000], ranging from ± 0.005 Sv to ± 0.2 Sv ($1\ \mathrm{Sv} = 10^6\ \mathrm{m}^3/\mathrm{s}$). The integration time for these experiments was long enough for the AMOC to reach a new equilibrium (500 years or longer if necessary, Figure S1 in the supporting information), which has been assessed by means of a *t* test.

In order to study the potential for bistability, the experiment with the strongest freshwater input of +0.2 Sv was subsequently continued after removing the freshwater perturbation. Recovery of the AMOC hints at a monostable MIS3 baseline AMOC [*Prange et al*., 2002]. All results presented in this paper refer to the last 100 year mean climate of each experiment, representing quasi-equilibrium conditions.

In all simulations, ozone and aerosol distributions were kept at preindustrial levels [*Otto-Bliesner et al*., 2006].

3. Results

The 38 ka B.P. baseline simulation results in a climate that is significantly colder than preindustrial (PI) with a maximum cooling of more than 24 K in annual mean surface temperature over the Laurentide ice sheet in North America (Figure 1a). The annual global mean surface temperature is 3.3 K lower than that in the PI run. As shown in Figure 1a, the high latitudes generally experience a stronger temperature decrease compared to lower latitudes. However, a region of positive surface temperature anomalies in the Nordic Seas indicates intense inflow of Atlantic water from the south in the MIS3 simulation. This supply of warm and salty water keeps large parts of the Nordic Seas ice free (Figure 1a) and maintains convection and deep water formation during winter. As a result, CCSM3 simulates a vigorous AMOC in the MIS3 baseline run with a North Atlantic overturning maximum of 15.4 Sv, which is ~1.5 Sv stronger than that in the PI control run (Figure 2). The southward flow of North Atlantic deep water occurs at shallower levels in the MIS3 run than under PI conditions.

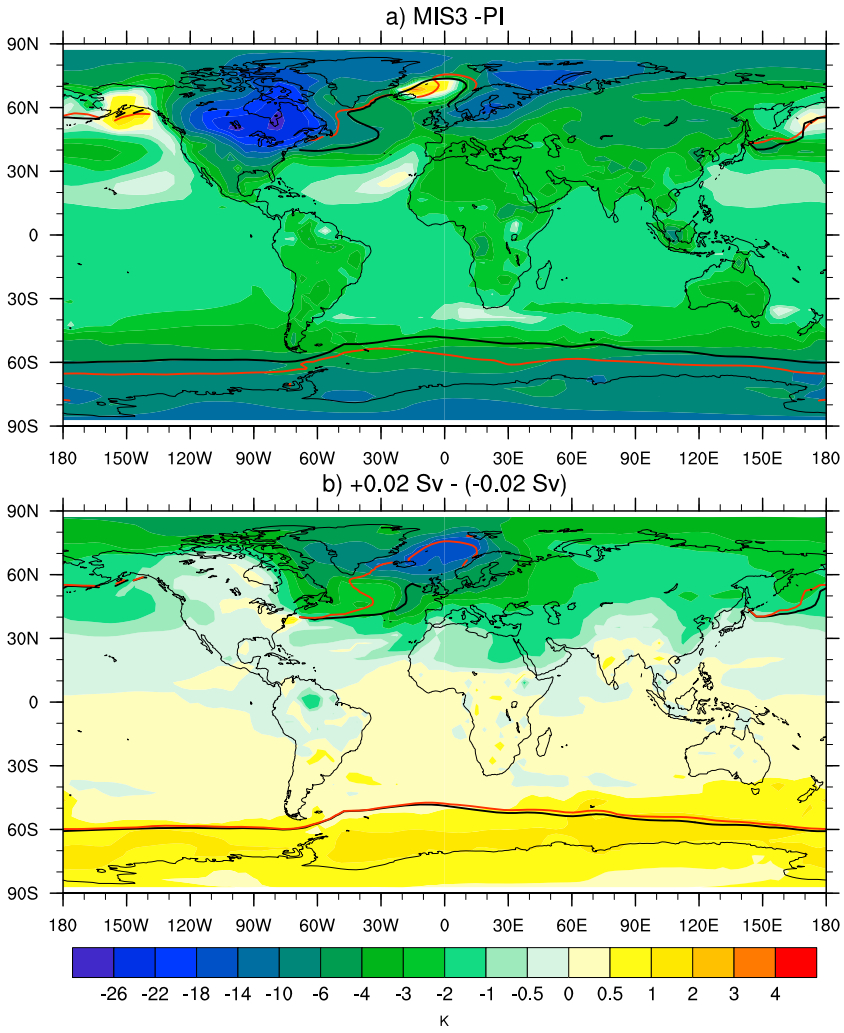

Figure 1. Annual mean surface temperature differences with winter (December–February mean) sea ice margins. (a) Difference between the MIS3 baseline simulation with 38 ka B.P. boundary conditions and the preindustrial control run. Black and red contour lines mark the winter sea ice margins (with 10% sea ice concentration) for the MIS3 and preindustrial simulations, respectively. (b) Difference between the MIS3 freshwater perturbation experiments with +0.02 Sv and −0.02 Sv forcing interpreted as stadial-interstadial climate difference. Black and red contour lines mark the winter sea ice margins for the +0.02 Sv and −0.02 Sv experiments, respectively. Note the irregular contour intervals.

We perturbed the AMOC in a series of freshwater-hosing/extraction experiments as described above. In almost all experiments, an integration time of 500 years was long enough for the meridional overturning stream function to reach a new equilibrium, only in one case the integration had to be extended (Figure S1). The AMOC equilibrium response to freshwater forcing in our set of experiments reveals the existence of a threshold by an abrupt drop in AMOC strength for North Atlantic freshwater forcing between −0.02 Sv and +0.02 Sv, with a particularly sensitive behavior between +0.01 Sv and +0.02 Sv (Figure 3a). Comparing the climatic states just above (+0.02 Sv perturbation; Figure 2c) and below (−0.02 Sv perturbation; Figure 2d) the threshold reveals a maximum cooling in the +0.02 Sv experiment over the Nordic Seas (Figure 1b) associated with an expansion of sea ice resulting in an increase of surface albedo and a decrease in ocean-atmosphere surface heat flux. In boreal winter, the sea ice margin in the North Atlantic is dramatically displaced to midlatitudes in response to the small positive freshwater forcing (Figure 1b). While the surface ocean experiences strongest cooling in the northern North Atlantic, subsurface temperatures increase in these regions (Figure S2).

In order to examine the AMOC for multiple equilibria, the +0.2 Sv experiment was continued without anomalous freshwater forcing (see section 2). Upon removal of the freshwater perturbation, the AMOC fully recovers, suggesting monostability of the MIS3 baseline AMOC (Figure S3).

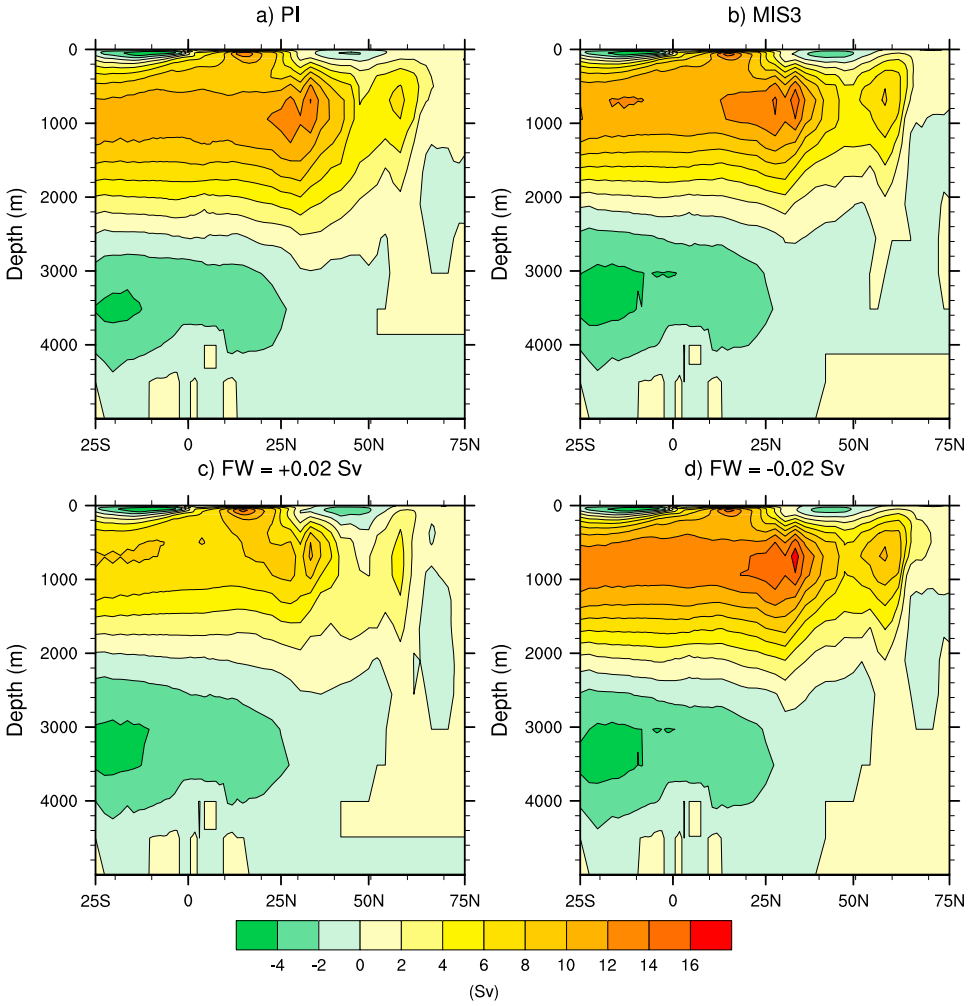

Figure 2. Meridional overturning stream function of the Atlantic Ocean (annual mean) in different experiments. (a) Preindustrial control run. (b) MIS3 baseline simulation. (c) MIS3 freshwater-hosing experiment with +0.02 Sv perturbation. (d) Freshwater extraction experiment with −0.02 Sv forcing. Positive values indicate clockwise circulation.

In summary, the MIS3 baseline state is very sensitive with respect to minor freshwater perturbations. A decrease (increase) to 10.6 Sv (17.2 Sv) of the AMOC strength in response to a weak positive (negative) freshwater forcing of 0.02 Sv is simulated (Figure 3a). The associated difference in oceanic heat transport between these two states with reduced and intensified AMOC leads to a pronounced interhemispheric "seesaw pattern" [*Stocker*, 1998; *Stocker and Johnsen*, 2003] in surface temperature (Figure 1b). More specifically, the annual mean surface temperature over central Greenland is about 8 K lower in the +0.02 Sv experiment compared to the −0.02 Sv run, while Antarctica warms by about 0.5–1 K, consistent with the difference between an interstadial and a stadial climate state [*EPICA community members*, 2006; *Huber et al.*, 2006].

4. Implications

Previous freshwater-hosing studies with comprehensive coupled climate models run under modern (interglacial) or Last Glacial Maximum (LGM; 21 ka B.P.) boundary conditions suggested a rather linear response of the AMOC to increasing freshwater perturbations without any obvious threshold effects [e.g., *Rind et al.*, 2001; *Otto-Bliesner and Brady*, 2010]. By contrast, the MIS3 AMOC stability diagram constructed from the set of our freshwater perturbation experiments reveals a pronounced threshold for anomalous freshwater forcing between −0.02 Sv and +0.02 Sv (Figure 3a). Consequently, the MIS3 baseline climate state is remarkably unstable with respect to minor freshwater perturbations which are an order of magnitude smaller than what is generally necessary to induce a substantial weakening of the AMOC and associated Greenland cooling in

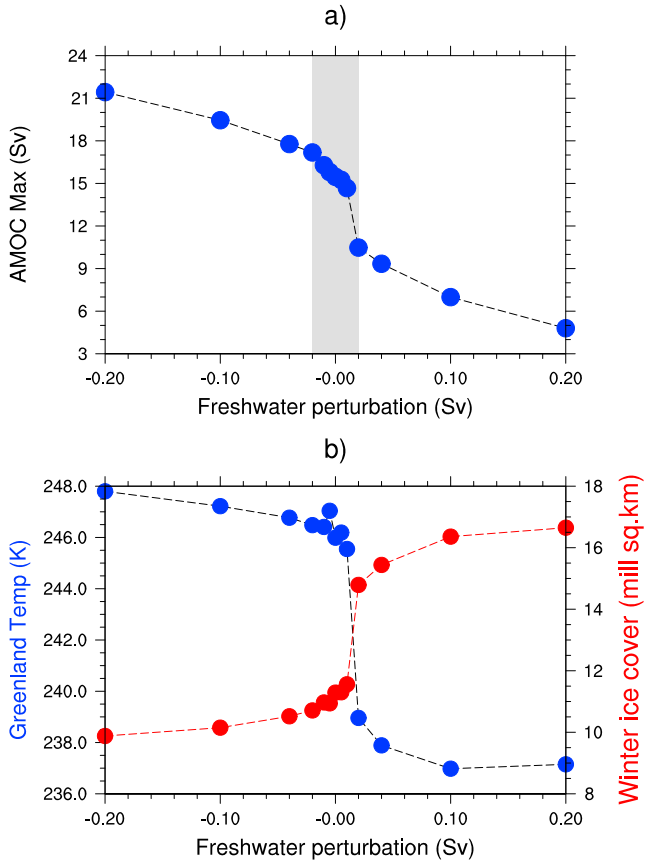

Figure 3. Modeled climate changes as a function of freshwater perturbation. (a) Strength of the equilibrated AMOC as a function of freshwater perturbation. The AMOC strength was defined as the maximum value of the overturning stream function below 300 m depth in the North Atlantic. Positive perturbations correspond to freshwater input to the Nordic Seas, whereas negative perturbations correspond to freshwater removal. The threshold between −0.02 Sv and +0.02 Sv is highlighted. (b) Annual mean central Greenland surface temperature (blue) and winter (December–February mean) sea ice area over the North Atlantic/Arctic Ocean (red) as a function of freshwater perturbation.

climate models under modern or glacial boundary conditions [*Rahmstorf et al.*, 2005; *Stouffer et al.*, 2006; *Valdes*, 2011; *Kageyama et al.*, 2013; *Gong et al.*, 2013; *Hopcroft et al.*, 2011] or what has been estimated as meltwater input during Heinrich events [*Hemming*, 2004].

In our MIS3 experiments, climate states below the freshwater perturbation threshold, with an AMOC strength of 16 Sv and more, are consistent with interstadial conditions, while climate states above the threshold, with an AMOC weaker than 11 Sv, correspond to stadial conditions. Our MIS3 baseline simulation yields an AMOC transport of about 15 Sv which is slightly stronger than in the PI control run. Previous MIS3 simulations using CCSM3 by *Merkel et al.* [2010] and *Brandefelt et al.* [2011] provided climate states with weaker North Atlantic overturning circulation of ~8 and ~11 Sv, respectively, and fully ice-covered Nordic Seas in winter, which have been interpreted as stadial climates in the absence of freshwater perturbations. Given the proximity of the MIS3 baseline climate to the AMOC stability threshold (Figure 3a), we conjecture that minor differences in the modeled hydrologic cycles compared to our baseline experiment resulted in the simulation of stadial MIS3 equilibrium states in these earlier studies. Such minor differences in the hydrologic cycles may be caused not only by the use of different MIS3 boundary conditions (including ice sheet distribution, greenhouse gas concentrations, and orbital parameters) and CCSM3 grid resolutions [*Brandefelt et al.*, 2011] but also by our modifications in the land model component including the implementation of interactive dynamic vegetation. Indeed, applying a negative freshwater forcing of −0.1 Sv to the MIS3 simulation of *Merkel et al.* [2010] resulted in a strengthening of the North Atlantic overturning to ~18 Sv [*Merkel et al.*, 2010], which is similar to the AMOC intensity in our −0.1 Sv freshwater extraction experiment (Figure 3a). As such, our new results are consistent with the earlier MIS3 simulations using CCSM3. However, due to the proximity of the MIS3 baseline climate state to the AMOC stability threshold, we infer that the unperturbed "typical near equilibrium" [*Van Meerbeeck et al.*, 2009] MIS3 climate cannot unequivocally be assigned to a stadial [*Merkel et al.*, 2010; *Brandefelt et al.*, 2011] or interstadial [*Van Meerbeeck et al.*, 2009] state.

For central Greenland, the simulated annual mean surface temperature difference between stadial and interstadial climates is 8–11 K (Figure 3b), in line with reconstructions from ice cores [*Huber et al.*, 2006; *Landais et al.*, 2004; *Kindler et al.*, 2014]. This temperature change over Greenland along with a concurrent anomaly in Antarctica of opposite sign is accomplished by relatively moderate changes in the AMOC in our CCSM3 experiments and lends further support to the bipolar seesaw concept as a characteristic of D-O events [*Stocker and Johnsen*, 2003]. Under modern boundary conditions, Greenland cooling larger than 6 K

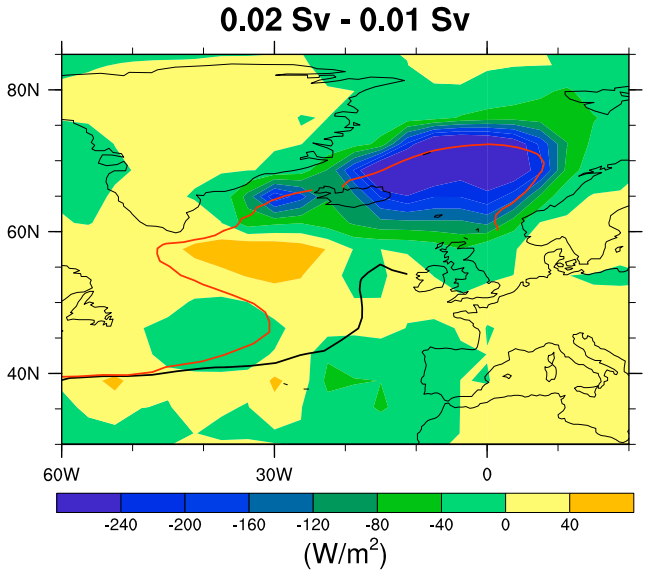

Figure 4. Winter (December–February mean) surface heat flux anomaly. Shown is the heat flux difference between the MIS3 freshwater-hosing experiment with +0.02 Sv forcing and the one with +0.01 Sv forcing. Positive values indicate upward heat flux into the atmosphere. Black and red contour lines mark the Northern Hemisphere winter sea ice margins for the +0.02 Sv and +0.01 Sv experiments, respectively.

can usually only be achieved with a complete AMOC shutdown that often requires strong freshwater forcing in the order of 1 Sv in coupled atmosphere-ocean models [*Stouffer et al.*, 2006]. Atmosphere general circulation model experiments [*Li et al.*, 2010] suggest that central Greenland surface temperature anomalies during D-O cycles are mainly controlled by winter sea ice coverage in the Nordic Seas. Our experiments strongly corroborate this finding (Figure 3b). Relatively warmer, interstadial conditions over Greenland are associated with reduced sea ice cover in the northern North Atlantic, with major ice-free areas in the Nordic Seas even during winter. By contrast, during cold, stadial conditions over Greenland, the winter sea ice margin shifts into the midlatitude North Atlantic. The most dramatic temperature drop over Greenland is found for freshwater perturbations between +0.01 Sv and +0.02 Sv accompanied by a substantial winter sea ice expansion (Figure 3b). A closer inspection of these two climate states reveals that the expansion of the winter sea ice cover in the experiment with +0.02 Sv freshwater forcing results in a reduction of the surface heat flux from the Nordic Seas to the overlying atmosphere by more than 240 W m^{-2} compared to the +0.01 Sv experiment (Figure 4), leading to a strong atmospheric cooling in that region during the winter months. The diabatic change is effectively distributed by wind and mixing around the Icelandic low, thereby affecting winter temperatures over the Greenland ice sheet [cf. *Li et al.*, 2010]. During winter, surface temperatures in central Greenland differ by ~10 K between the two experiments (not shown), whereas the difference in summer temperatures is minor (~2 K).

The close relationship between Nordic Seas' winter sea ice cover and central Greenland temperature is also evident from the transient behavior in the AMOC recovery experiment (Figure S3). More specifically, Greenland temperature rise (and fall) can occur at a much faster rate than changes in the AMOC strength (Figure S3). Once the AMOC strength and its associated heat transport become large enough to substantially melt the sea ice, Greenland temperature increase follows the sea ice decline. However, the rise in Greenland temperature occurs on a centennial scale in our model experiment, which is significantly longer than the multidecadal timescale suggested by ice core temperature reconstructions [e.g., *Thomas et al.*, 2009; *Kindler et al.*, 2014]. Whether this difference in timescales points to deficient (i.e., missing negative) freshwater forcing in the AMOC recovery experiment, to unresolved or missing processes in the climate model, or to a local character of ice core reconstructions is beyond the scope of our study. Paleoceanographic data from the Nordic Seas indeed suggest ice-covered conditions during MIS3 stadials, while open-ocean convection requiring ice-free conditions has been inferred for MIS3 interstadials [*Dokken and Jansen*, 1999; *Rasmussen and Thomsen*, 2004]. Once the AMOC is weak enough (~10 Sv, i.e., above the freshwater flux threshold) and the Nordic Seas are fully ice covered, further weakening of the AMOC has little effect on additional Greenland cooling (Figure 3b), similar to results found by *Ganopolski and Rahmstorf* [2001] in their CLIMBER-2 experiments. This behavior is consistent with paleoceanographic and paleoclimatic evidence, suggesting that an equivalent degree of cooling over Greenland was obtained during MIS3 stadials with different perturbations of deep-water formation [*Elliot et al.*, 2002].

The sea ice coverage in the northern North Atlantic, in turn, is linked to the strength of the AMOC. With weaker AMOC, less heat is transported by the ocean toward the north resulting in a southward displaced sea ice margin. A larger sea ice cover, on the other hand, inhibits convection and deep-water formation, thus

acting as a positive feedback to the slow down of the AMOC as pointed out by *Lohmann and Gerdes* [1998]. Coverage of convective sites by expanding sea ice may therefore induce nonlinearity in the relationship between AMOC strength and freshwater perturbation. Shutdown of convection in the ice-covered Nordic Seas is the principal cause for the AMOC weakening in the stadial climate (cf. Figure S4), similar to the key process in the EMIC study by *Ganopolski and Rahmstorf* [2001]. An important role for sea ice in abrupt millennial-scale climate change has also been suggested in previous studies [*Broecker*, 2000; *Timmermann et al*., 2003; *Clement and Peterson*, 2008; *Montoya and Levermann*, 2008; *Banderas et al*., 2012; *Li et al*., 2010; *Gildor and Tziperman*, 2003; *Loving and Vallis*, 2005; *Oka et al*., 2012].

In line with paleoceanographic evidence from the northern North Atlantic [*Rasmussen and Thomsen*, 2004; *Marcott et al*., 2011], our simulated stadial states exhibit large-scale subsurface oceanic warming in high northern latitudes (Figure S2). It has been suggested that such subsurface warming during surface cold phases, in particular, in the northwestern Atlantic, may have destabilized adjacent ice shelves, thus triggering ice stream surges and producing massive iceberg discharge from the Laurentide ice sheet, referred to as Heinrich events, which would have led to further weakening of the AMOC [*Marcott et al*., 2011; *Shaffer et al*., 2004; *Álvarez-Solas et al*., 2011]. This scenario may provide a plausible mechanism for the coincidence of Heinrich events with D-O stadial phases.

Despite the existence of a distinct threshold in the AMOC stability diagram (Figure 3a), we did not find evidence for the existence of multiple stable states under MIS3 boundary conditions in our simple AMOC recovery experiment. However, the existence of a narrow hysteresis, as in the EMIC study by *Ganopolski and Rahmstorf* [2001], cannot be ruled out. Whether the AMOC can generally possess multiple equilibria is an open question. It has been argued that bistability and associated irreversibility may be model dependent [e.g., *Ferreira et al*., 2011; *Hu et al*., 2013], or model artifacts due to missing atmospheric feedbacks [*Yin et al*., 2006], or erroneous subgrid-scale parameterizations in the ocean [*Prange et al*., 2003; *Nof et al*., 2007].

Ice sheets have often been considered an important component of D-O dynamics. Records of ice-rafted debris indicating enhanced iceberg and hence freshwater fluxes into the Nordic Seas during each D-O stadial [*Elliot et al*., 2002; *Dokken and Jansen*, 1999; *Voelker et al*., 1998]—possibly related to internal coastal ice sheet dynamics in east Greenland [*van Kreveld et al*., 2000] and/or Fennoscandia [*Elliot et al*., 2001]—support the notion that ice sheets played a role in producing the small positive freshwater flux anomalies that are required for crossing the AMOC stability threshold and thus to trigger D-O climate shifts. During interstadials, accumulation rates on continental ice sheets increased [*Andersen et al*., 2006; *Thomas et al*., 2009], possibly leading to a positive ice sheet mass balance and net freshwater removal from the high-latitude northern ocean causing a negative freshwater forcing to the AMOC [*Jackson et al*., 2010].

5. Conclusions

The stability properties of the AMOC and associated climate impacts have been investigated systematically using a coupled general circulation model under MIS3 boundary conditions. We found that the MIS3 baseline climate is remarkably unstable such that minor North Atlantic freshwater perturbations in the order of 0.02 Sv can trigger dramatic changes in the strength of Atlantic overturning, leading to stadial-interstadial climate anomalies. The close linkage between North Atlantic sea ice area and AMOC strength suggests a key role for sea ice in the instability of the AMOC. In addition, strong variations in Nordic Seas winter ice extent appear crucial for large D-O-type temperature anomalies (8–11 K in the annual average) in central Greenland, which is difficult to simulate when inappropriate (e.g., modern) boundary conditions are used in freshwater-hosing experiments. According to our model results, minor perturbations in the hydrologic cycle—possibly connected with ice sheet dynamics—could have triggered substantial global D-O climate transitions. Even though the CCSM3 results are to a large extent consistent with earlier findings from an EMIC study [*Ganopolski and Rahmstorf*, 2001], further MIS3 climate stability experiments with different state-of-the-art coupled general circulation models are required in order to assess the robustness of these results.

Acknowledgments

The authors thank Stefan Rahmstorf, Andrey Ganopolski, and an anonymous reviewer for helpful comments that substantially improved the manuscript. This work has received funding through the DFG Research Center/Cluster of Excellence "The Ocean in the Earth System" at the University of Bremen. The CCSM3 climate model experiments were run on the SGI Altix Supercomputer of the "Norddeutscher Verbund für Hoch- und Höchstleistungsrechnen" (HLRN). Data are available at PANGAEA.

The Editor thanks two anonymous reviewers for assistance in evaluating this paper.

References

Ahn, J., and E. J. Brook (2007), Atmospheric CO_2 and climate from 65 to 39 ka BP, *Geophys. Res. Lett.*, *34*, L10703, doi:10.1029/2007GL029551.

Álvarez-Solas, J., et al. (2011), Heinrich event 1: An example of dynamical ice-sheet reaction to oceanic changes, *Clim. Past*, *7*, 1297–1306.

Andersen, K. K., et al. (2006), The Greenland Ice Core Chronology 2005, 15–42 ka. Part 1: Constructing the time scale, *Quat. Sci. Rev.*, *25*, 3246–3257.

Banderas, R., J. Álvarez-Solas, and M. Montoya (2012), Role of CO_2 and Southern Ocean winds in glacial abrupt climate change, *Clim. Past*, *8*, 1011–1021, doi:10.5194/cp-8-1011-2012.
Bereiter, B., D. Lüthi, M. Siegrist, S. Schüpbach, T. F. Stocker, and H. Fischer (2012), Mode change of millennial CO_2 variability during the last glacial cycle associated with a bipolar marine carbon seesaw, *Proc. Natl. Acad. Sci. U.S.A.*, *109*, 9755–9760.
Berger, A. (1978), Long term variations of daily insolation and Quaternary climatic changes, *J. Atmos. Sci.*, *35*(2), 2362–2367.
Bond, G., W. Broecker, S. Johnsen, J. McManus, L. Labeyrie, J. Jouzel, and G. Bonani (1993), Correlations between climate records from North Atlantic sediments and Greenland ice, *Nature*, *365*, 143–147.
Brandefelt, J., E. Kjellström, J.-O. Näslund, G. Strandberg, A. H. L. Voelker, and B. Wohlfarth (2011), A coupled climate model simulation of Marine Isotope Stage 3 stadial climate, *Clim. Past*, *7*, 649–670.
Broecker, W. S. (2000), Abrupt climate change: Causal constraints provided by the paleoclimate record, *Earth Sci. Rev.*, *51*, 137–154.
Clement, A. C., and L. C. Peterson (2008), Mechanisms of abrupt climate change of the last glacial period, *Rev. Geophys.*, *46*, RG4002, doi:10.1029/2006RG000204.
Colin de Verdière, A. M., J. Ben, and F. Sévellec (2006), Bifurcation structure of thermohaline millennial oscillations, *J. Climate*, *19*, 5777–5795.
Collins, D. W., et al. (2006), The Community Climate System Model Version 3 (CCSM3), *J. Climate*, *19*, 2122–2143.
Dansgaard, W., et al. (1993), Evidence for general instability of past climate from a 250-kyr ice-core record, *Nature*, *364*, 218–220.
Dokken, T. M., and E. Jansen (1999), Rapid changes in the mechanism of ocean convection during the last glacial period, *Nature*, *401*, 458–461.
Elliot, M., L. Labeyrie, T. Dokken, and S. Manthé (2001), Coherent patterns of ice-rafted debris deposits in the Nordic regions during the last glacial (10–60 ka), *Earth Planet. Sci. Lett.*, *194*, 151–163.
Elliot, M. L., L. Labeyrie, and J. C. Duplessy (2002), Changes in North Atlantic deep-water formation associated with the Dansgaard-Oeschger temperature oscillations (60–10 ka), *Quat. Sci. Rev.*, *21*(10), 1153–1165.
EPICA Community Members (2006), One-to-one coupling of glacial climate variability in Greenland and Antarctica, *Nature*, *444*, 195–198.
Ferreira, D., J. Marshall, and B. Rose (2011), Climate determinism revisited: Multiple equilibria in a complex climate model, *J. Climate*, *24*(4), 992–1012.
Flückiger, J., T. Blunier, B. Stauffer, J. Chappellaz, R. Spahni, K. Kawamura, J. Schwander, T. F. Stocker, and D. Dahl-Jensen (2004), N_2O and CH_4 variations during the last glacial epoch: Insight into global processes, *Global Biogeochem. Cycles*, *18*, GB1020, doi:10.1029/2003GB002122.
Ganopolski, A., and S. Rahmstorf (2001), Rapid changes of glacial climate simulated in a coupled climate model, *Nature*, *409*, 153–158.
Gildor, H., and E. Tziperman (2003), Sea-ice switches and abrupt climate change, *Philos. Trans. R. Soc. London Ser. A*, *361*, 1935–1942.
Gong, X., G. Knorr, and G. Lohmann (2013), Dependence of abrupt Atlantic meridional ocean circulation changes on climate background states, *Geophys. Res. Lett.*, *40*, 3691–3704, doi:10.1002/grl.50701.
Handiani, D., A. Paul, M. Prange, U. Merkel, L. Dupont, and X. Zhang (2013), Tropical vegetation response to Heinrich Event 1 as simulated with the UVic ESCM and CCSM3, *Clim. Past*, *9*, 1683–1696, doi:10.5194/cp-9-1683-2013.
Hemming, S. R. (2004), Heinrich events: Massive late Pleistocene detrius layers of the North Atlantic and their global climate imprint, *Rev. Geophys.*, *42*, RG1005, doi:10.1029/2003RG000128.
Hopcroft, P. O., P. J. Valdes, and D. J. Beerling (2011), Simulating idealized Dansgaard-Oeschger events and their potential impacts on the global methane cycle, *Quat. Sci. Rev.*, *30*, 3258–3268.
Hu, A., G. A. Meehl, W. Han, J. Lu, and W. G. Strand (2013), Energy balance in a warm world without the ocean conveyor belt and sea ice, *Geophys. Res. Lett.*, *40*, 6242–6246, doi:10.1002/2013GL058123.
Huber, C., M. Leuenberger, R. Spahni, J. Flückiger, J. Schwander, T. F. Stocker, S. Johnsen, A. Landais, and J. Jouzel (2006), Isotope calibrated Greenland temperature record over Marine Isotope Stage 3 and its relation to CH_4, *Earth Planet. Sci. Lett.*, *243*, 504–519.
Jackson, C. S., O. Marchal, Y. Liu, S. Lu, and W. G. Thompson (2010), A box model test of the freshwater forcing hypothesis of abrupt climate change and the physics governing ocean stability, *Paleoceanography*, *25*, PA4222, doi:10.1029/2010PA001936.
Kageyama, M., et al. (2013), Climatic impacts of fresh water hosing under Last Glacial Maximum conditions: A multi-model study, *Clim. Past*, *9*, 935–953.
Keigwin, L. D., and E. A. Boyle (1999), Surface and deep ocean variability in the northern Sargasso Sea during marine isotope stage 3, *Paleoceanography*, *14*, doi:10.1029/1998PA900026.
Kindler, P., M. Guillevic, M. Baumgartner, J. Schwander, A. Landais, and M. Leuenberger (2014), Temperature reconstruction from 10 to 120 kyr b2k from the NGRIP ice core, *Clim. Past*, *10*, 887–902.
Knorr, G., and G. Lohmann (2003), Southern ocean origin for the resumption of Atlantic thermohaline circulation during deglaciation, *Nature*, *424*, 532–536.
Landais, A., N. Caillon, C. Goujon, A. M. Grachev, J. M. Barnola, J. Chappellaz, J. Jouzel, V. Masson-Delmotte, and M. Leuenberger (2004), Quantification of rapid temperature change during DO event 12 and phasing with methane inferred from air isotopic measurements, *Earth Planet. Sci. Lett.*, *225*, 221–232.
Levis, S., et al. (2004), The community land model's dynamic global vegetation model (CLM-DGVM): Technical description and user's guide, NCAR Technical Note NCAR/TN-459 + STR, 50 pp., National Center for Atmospheric Research, Boulder, Colo.
Li, C., D. S. Battisti, and C. M. Bitz (2010), Can North Atlantic sea ice anomalies account for Dansgaard–Oeschger climate signals?, *J. Climate*, *23*, 5457–5475.
Lohmann, G., and R. Gerdes (1998), Sea ice effects on the sensitivity of the thermohaline circulation in simplified atmosphere-ocean-sea ice models, *J. Climate*, *11*, 2789–2803.
Loving, J. L., and G. K. Vallis (2005), Mechanisms for climate variability during glacial and interglacial periods, *Paleoceanography*, *20*, PA4024, doi:10.1029/2004PA001113.
Marcott, S. A., et al. (2011), Ice-shelf collapse from subsurface warming as a trigger for Heinrich events, *Proc. Natl. Acad. Sci. U.S.A.*, *108*, 13,415–13,419.
Merkel, U., M. Prange, and M. Schulz (2010), ENSO variability and teleconnections during glacial climates, *Quat. Sci. Rev.*, *29*, 86–100.
Montoya, M., and A. Levermann (2008), Surface wind-stress threshold for glacial Atlantic overturning, *Geophys. Res. Lett.*, *35*, L03608, doi:10.1029/2007GL032560.
Nof, D., S. Van Gorder, and A. M. De Boer (2007), Does the Atlantic meridional overturning cell really have more than one stable steady state?, *Deep Sea Res., Part I*, *54*(11), 2005–2021.
Oka, A., H. Hasumi, and A. Abe-Ouchi (2012), The thermal threshold of the Atlantic meridional overturning circulation and its control by wind stress forcing during glacial climate, *Geophys. Res. Lett.*, *39*, L09707, doi:10.1029/2012GL051421.
Oleson, K. W., et al. (2004), Technical description of the Community Land Model (CLM), NCAR Technical Note NCAR/TN-461 + STR, 173 pp., National Center for Atmospheric Research, Boulder, Colo.
Oleson, K. W., et al. (2008), Improvements to the Community Land Model and their impact on the hydrological cycle, *J. Geophys. Res.*, *113*, G01021, doi:10.1029/2007JG000563.

Otto-Bliesner, B. L., and E. C. Brady (2010), The sensitivity of the climate response to the magnitude and location of freshwater forcing: Last glacial maximum experiments, *Quat. Sci. Rev.*, *29*, 56–73.
Otto-Bliesner, B., E. C. Brady, G. Clauzet, R. Tomas, S. Levis, and Z. Kothavala (2006), Last glacial maximum and Holocene climate in CCSM3, *J. Climate*, *19*, 2526–2544.
Peltier, W. R. (2004), Global glacial isostasy and the surface of the ice-age Earth: The ICE-5G (VM2) model and GRACE, *Annu. Rev. Earth Planet. Sci.*, *32*, 111–149.
Prange, M., and R. Gerdes (2006), The role of surface freshwater flux boundary conditions in Arctic Ocean modelling, *Ocean Model.*, *13*, 25–43.
Prange, M., V. Romanova, and G. Lohmann (2002), The glacial thermohaline circulation: Stable or unstable?, *Geophys. Res. Lett.*, *29*(21), 2028, doi:10.1029/2002GL015337.
Prange, M., G. Lohmann, and A. Paul (2003), Influence of vertical mixing on the thermohaline hysteresis: Analyses of an OGCM, *J. Phys. Oceanogr.*, *33*(8), 1707–1721.
Rahmstorf, S., et al. (2005), Thermohaline circulation hysteresis: A model intercomparison, *Geophys. Res. Lett.*, *32*, L23605, doi:10.1029/2005GL023655.
Rasmussen, T. L., and E. Thomsen (2004), The role of the North Atlantic Drift in the millennial timescale glacial climate fluctuations, *Palaeogeogr. Palaeoclimatol. Palaeoecol.*, *210*, 101–116.
Rind, D., et al. (2001), Effects of glacial meltwater in the GISS coupled atmosphere-ocean model: 1. North Atlantic deep water response, *J. Geophys. Res.*, *106*(D21), 27,335–27,353, doi:10.1029/2000JD000070.
Sarnthein, M., et al. (2001), Fundamental modes and abrupt changes in North Atlantic circulation and climate over the last 60 ky—Concepts, reconstructions and numerical modeling, in *The Northern North Atlantic: A Changing Environment*, edited by P. Schäfer et al., pp. 365–410, Springer-Verlag, New York.
Schmittner, A., M. Yoshimori, and A. J. Weaver (2002), Instability of glacial climate in a model of the ocean-atmosphere-cryosphere system, *Science*, *295*, 1489–1493.
Schulz, M. (2002), On the 1470-year pacing of Dansgaard-Oeschger warm events, *Paleoceanography*, *17*(2), doi:10.1029/2000PA000571.
Shaffer, G., S. O. Malskaer, and C. J. Bjerrum (2004), Ocean subsurface warming as a mechanism for coupling Dansgaard-Oeschger climate cycles and ice-rafting events, *Geophys. Res. Lett.*, *31*, L24202, doi:10.1029/2004GL020968.
Spahni, R., et al. (2005), Atmospheric methane and nitrous oxide of the late Pleistocene from Antarctic ice cores, *Science*, *310*, 1317–1321.
Stocker, T. F. (1998), The seesaw effect, *Science*, *282*, 61–62.
Stocker, T. F., and S. J. Johnsen (2003), A minimum thermodynamic model for the bipolar seesaw, *Paleoceanography*, *18*(4), 1087, doi:10.1029/2003PA000920.
Stocker, T. F., and D. G. Wright (1991), Rapid transitions of the ocean's deep circulation induced by changes in the surface water fluxes, *Nature*, *351*, 729–732.
Stouffer, R. J., et al. (2006), Investigating the causes of the response of the thermohaline circulation to past and future climate changes, *J. Climate*, *19*, 1365–1387.
Thomas, E. R., et al. (2009), Anatomy of a Dansgaard-Oeschger warming transition: High-resolution analysis of the North Greenland Ice Core Project ice core, *J. Geophys. Res.*, *114*, D08102, doi:10.1029/2008JD011215.
Timmermann, A., H. Gildor, M. Schulz, and E. Tziperman (2003), Coherent resonant millennial-scale climate oscillations triggered by massive meltwater pulses, *J. Climate*, *16*, 2569–2585, doi:10.1175/1520-0442(2003)016<2569:CRMCOT>2.0.CO;2.
Valdes, P. (2011), Built for stability, *Nat. Geosci.*, *4*(7), 414–416.
van Kreveld, S. A., M. Sarnthein, H. Erlenkeuser, P. Grootes, S. Jung, M. J. Nadeau, U. Pflaumann, and A. Voelker (2000), Potential links between surging ice sheets, circulation changes, and the Dansgaard-Oeschger cycles in the Irminger Sea, 60–18 kyr, *Paleoceanography*, *15*(4), doi:10.1029/1999PA000464.
Van Meerbeeck, C. J., H. Renssen, and D. M. Roche (2009), How did Marine Isotope Stage 3 and Last Glacial Maximum climates differ?—Perspectives from equilibrium simulations, *Clim. Past*, *5*, 33–51.
Voelker, A. H. L., and workshop participants (2002), Global distribution of centennial-scale records for marine isotope state (MIS) 3: A database, *Quat. Sci. Rev.*, *21*, 1185–1214.
Voelker, A. H. L., M. Sarnthein, P. M. Grootes, H. Erlenkeuser, C. Laj, A. Mazaud, M. J. Nadeau, and M. Schleicher (1998), Correlation of marine ^{14}C ages from the Nordic Seas with the GISP2 isotope record: Implications for ^{14}C calibration beyond 25 ka BP, *Radiocarbon*, *40*(1), 517–34.
Yeager, S. G., C. A. Shields, W. G. Large, and J. J. Hack (2006), The low-resolution CCSM3, *J. Climate*, *19*, 2545–2566.
Yin, J., M. E. Schlesinger, N. G. Andronova, S. Malyshev, and B. Li (2006), Is a shutdown of the thermohaline circulation irreversible?, *J. Geophys. Res.*, *111*, D12104, doi:10.1029/2005JD006562.

Auxiliary Material for

Instability of the Atlantic overturning circulation during Marine Isotope Stage 3.

Xiao Zhang[1], Matthias Prange[1], Ute Merkel[1], Michael Schulz[1]

[1]MARUM – Center for Marine Environmental Sciences and Faculty of Geosciences, University of Bremen, Klagenfurter Str., 28334 Bremen, Germany

Geophysical Research Letters

Four supplementary figures from all freshwater experiments. Detailed figure captions are as follows:

Fig. S1. Time series of the maximum in the annual-mean North Atlantic overturning streamfunction (below 300 m). The last 500 years of the MIS3 control run (top) and the twelve freshwater hosing (left) and extraction (right) experiments were plotted. Starting at model year 3170 (see experimental design) each experiment was run for 500 years. From the last 100 years of each experiment, the trend in the overturning time series was calculated based on linear regression and statistical significance at the 0.05 level was assessed via a Student t-test. Only in case the null hypothesis (being that there is no trend) was rejected the experiment was continued until the trend disappeared (again assessed by a t-test based on 100 years linear regression). A continuation was only necessary for the -0.01 Sv experiment.

Fig. S2. Annual-mean ocean temperature differences between the MIS3 freshwater perturbation experiments with +0.02 Sv and -0.02 Sv forcing. a, Sea surface. **b**, 148 m depth. **c**, 326 m depth. The differences are interpreted as stadial-interstadial climate anomalies.

Fig. S3. Continuation of the 500-year long +0.2 Sv freshwater-hosing experiment after removal of the freshwater perturbation. Shown is the time series of the maximum in the annual-mean North Atlantic overturning streamfunction (below 300 m) along with annual-mean central Greenland surface temperature and winter sea-ice area over the North Atlantic/Arctic Ocean. The red line marks the end of the water hosing.

Fig. S4. Annual-mean mixed layer depths. a, MIS3 freshwater perturbation experiment with +0.02 Sv forcing (stadial climate). **b,** MIS3 freshwater perturbation experiment with -0.02 Sv forcing (interstadial climate). The mixed layer depths reveal shutdown of convection in the Nordic Seas in the stadial climate state.

Fig. S1

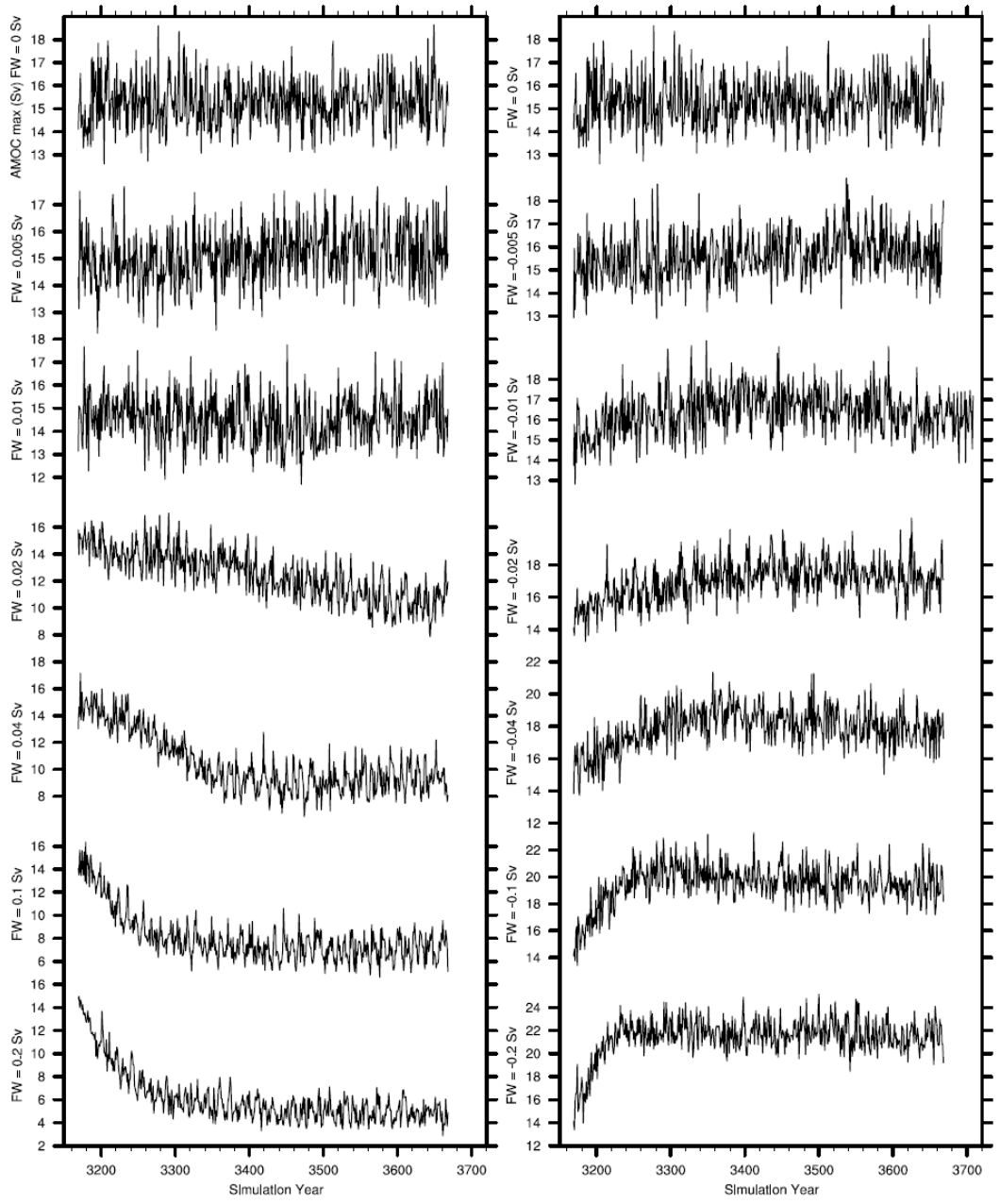
AMOC max (Sv) FW = 0 Sv
FW = 0.005 Sv
FW = 0.01 Sv
FW = 0.02 Sv
FW = 0.04 Sv
FW = 0.1 Sv
FW = 0.2 Sv
FW = 0 Sv
FW = -0.005 Sv
FW = -0.01 Sv
FW = -0.02 Sv
FW = -0.04 Sv
FW = -0.1 Sv
FW = -0.2 Sv
3200
3300
3400
3500
3600
3700
Simulation Year
Simulation Year

Fig. S2

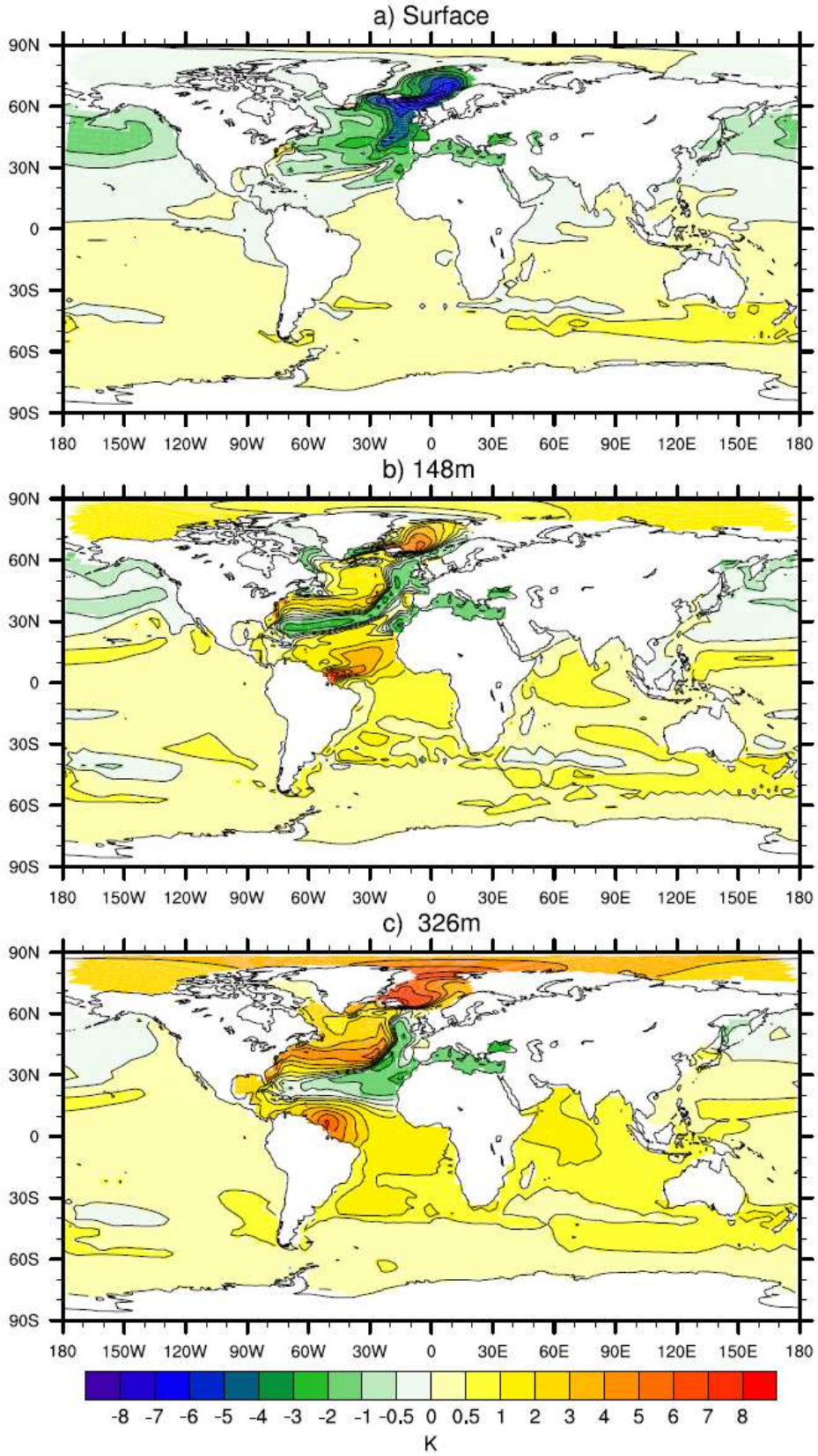
a) Surface
b) 148m
c) 326m
90N
60N
30N
0
30S
60S
90S
180 150W 120W 90W 60W 30W 0 30E 60E 90E 120E 150E 180
-8 -7 -6 -5 -4 -3 -2 -1 -0.5 0 0.5 1 2 3 4 5 6 7 8
K

Fig. S3

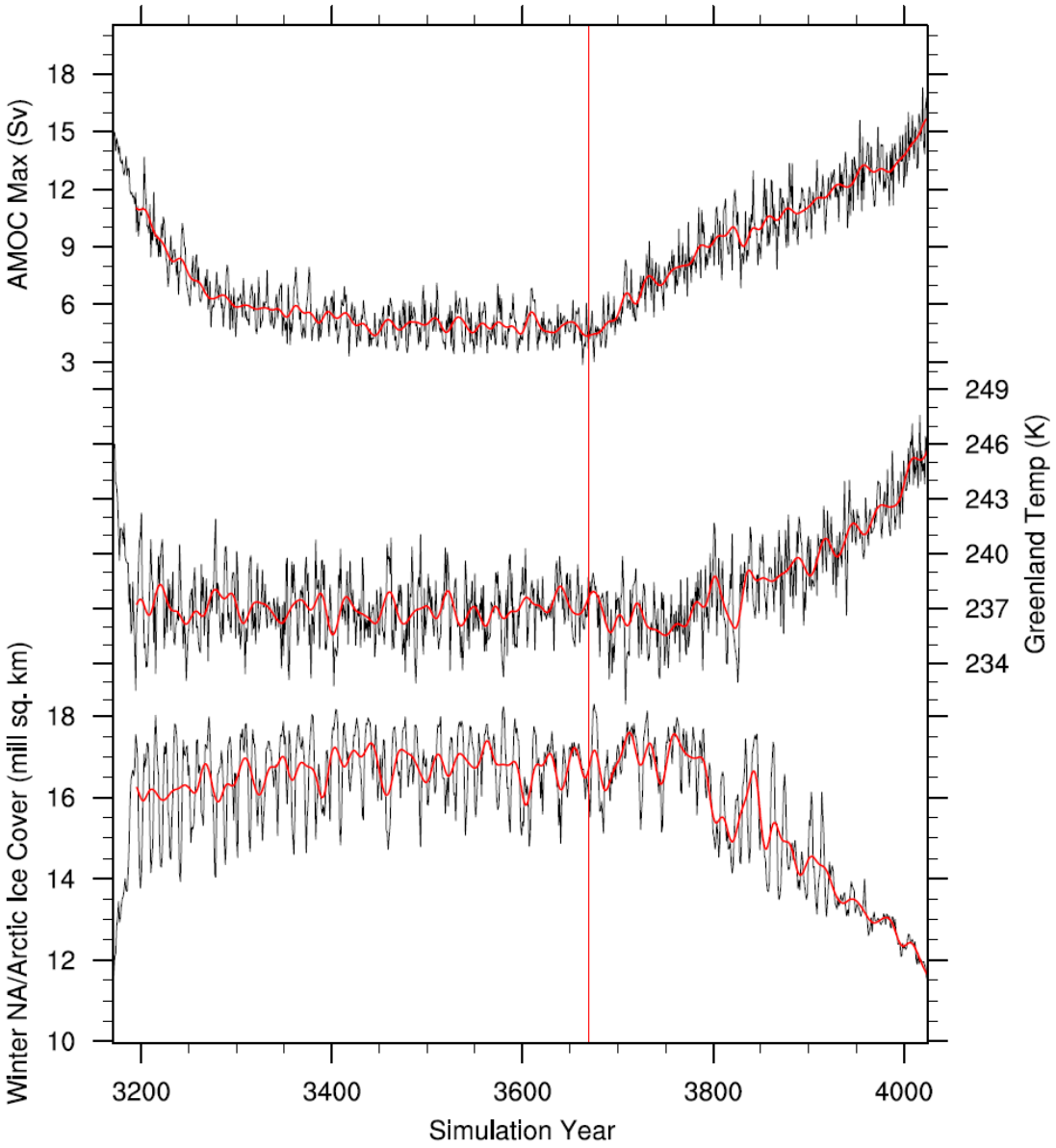
AMOC Max (Sv)
18
15
12
9
6
3
Greenland Temp (K)
249
246
243
240
237
234
Winter NA/Arctic Ice Cover (mill sq. km)
18
16
14
12
10
3200
3400
3600
3800
4000
Simulation Year

Fig.S4

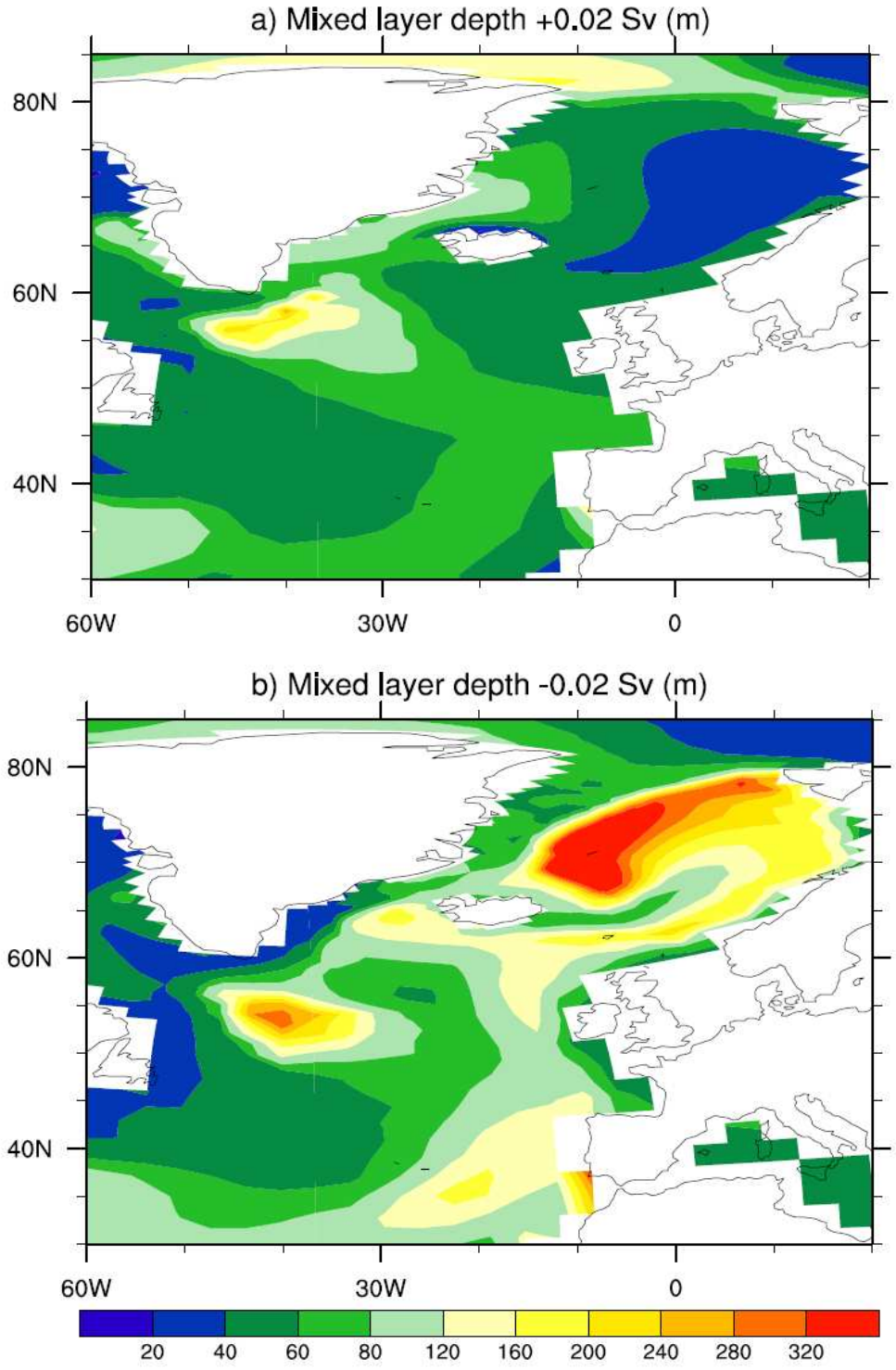
a) Mixed layer depth +0.02 Sv (m)
80N
60N
40N
60W
30W
0
b) Mixed layer depth -0.02 Sv (m)
80N
60N
40N
60W
30W
0
20
40
60
80
120
160
200
240
280
320